Nanoscale

Accepted Manuscript

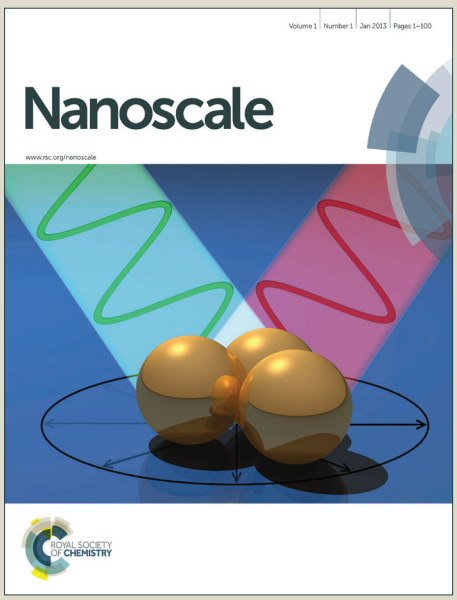

ROYAL SOCIETY OF CHEMISTRY

www.rsc.org/nanoscale

Nanoscale

RSCPublishing

PAPER

Multi-functional quantum dot-polypeptide hybrid nanogel for targeted imaging and drug delivery

Cite this: DOI: 10.1039/x0xx00000x

Jie Yang, Ming-Hao Yao, Lang Wen, Ji-Tao Song, Ming-Zhen Zhang, Yuan-Di Zhao*, Bo Liu*

Received 00th January 2014,
Accepted 00th January 2014

DOI: 10.1039/x0xx00000x

www.rsc.org/

A new type of multi-functional quantum dot (QD)-polypeptide hybrid nanogel with targeted imaging and drug delivery properties has been developed by metal-affinity driven self-assembly between artificial polypeptide and CdSe-ZnS core-shell QDs. On the surface of QDs, a tunable sandwich-like microstructure consisting of two hydrophobic layers and one hydrophilic layer between them were verified by capillary electrophoresis, transmission electron microscopy, and dynamic light scattering measurements. Hydrophobic and hydrophilic drugs can be loaded simultaneously in QD-polypeptide nanogel. *In vitro* drug release of drug-loaded QD-polypeptide nanogels varies strongly with temperature, pH, and competitor. Drug-loaded QD-polypeptide nanogel with an arginine-glycine-aspartic acid (RGD) motif exhibited efficient receptor-mediated endocytosis in $\alpha_v\beta_3$ overexpressing HeLa cells but not in the control MCF-7 cells as analyzed by confocal microscopy and flow cytometry. In contrast, non-targeted QD-polypeptide nanogels revealed minimal binding and uptake in HeLa cells. Compared with the original QDs, the QD-polypeptide nanogels showed lower *in vitro* cytotoxicity for both HeLa cells and NIH 3T3 cells. Furthermore, cytotoxicity of the targeted QD-polypeptide nanogel was lower for normal NIH 3T3 cells than that for HeLa cancer cells. These results demonstrate that the integration of imaging and drug delivery functions in a single QD-polypeptide nanogel has the potential application in cancer diagnosis, imaging, and therapy.

Introduction

Multi-functional nanocarrier systems have been explored for various biomedical applications in recent years due to the unique properties of nano-scale matter, the diversity of available materials, and infinite design schemes. A major advantage of multi-functional nanocarriers over other systems is that they can potentially combine several functionalities, such as imaging, drug delivery, and therapy in a single unit.[1, 2] For example, the combination of detection of malignant cells with targeted delivery of therapeutically active drugs in a nanocarrier unit is usually designed and applied for cancer therapy.[3, 4] Targeted nanocarriers with therapeutic drugs can increase the amount of drug that reaches a tumor and decrease the amount of drug that harms healthy tissue. Quantum dots (QDs) have been widely studied as luminescent probes in biomedical applications due to their advantages of broad excitation and narrow emission spectra, superior brightness, photostability, and tunable emission wavelength compared to conventional organic dyes.[5] Current applications include deep-tissue and tumor imaging, intracellular sensors, sensitizers for photodynamic therapy. These applications all require the delivery of QDs into the targeted cells.[6-8] Some strategies involving the cellular uptake of QDs such as fluid-phase, receptor-mediated endocytosis have been developed in several animal models.[9, 10] Lieleg et al. used the specific interaction of the tripeptide arginine-glycine-aspartic acid (RGD) with heterodimeric cell surface receptors to facilitate the QDs delivery.[11] In addition to the peptide-mediated QDs delivery, proteins (epidermal growth factor, transferrin, antibodies, and cholera toxin B) modified QDs were also reported to recognize and bind with a specific receptor or marker.[12-14] However, the applications of QDs in nanomedicine are still limited due to their high toxicity and lack of therapeutic functions.

QDs are very promising in building multi-functional nanocarriers for drug delivery because of their versatile surface chemistry, high capacity, and high stability. To date, two major strategies have been developed for drug delivery applications. One strategy is to utilize QDs as fluorescent markers for tagging conventional drug carriers.[15, 16] For example, QDs conjugated on external or encapsulated in functionalized polyethylene glycol-lipid as the hybrid vesicles in the

Britton Chance Center for Biomedical Photonics at Wuhan National Laboratory for Optoelectronics–Hubei Bioinformatics & Molecular Imaging Key Laboratory, Department of Biomedical Engineering, College of Life Science and Technology, Huazhong University of Science and Technology, Wuhan 430074, P. R. China. Fax: 86 27 87792202; Tel: 86 27 87792235; E-mail: zydi@mail.hust.edu.cn (Y.-D. Zhao), lbyang@mail.hust.edu.cn (B. Liu)

†Electronic Supplementary Information (ESI) available: See DOI: 10.1039/b000000x/

solid tumor tissue of tumor-bearing mice were reported.[15] The other strategy is to load drug on the surface of QDs via covalent coupling or electrostatic interaction.[17, 18] Compared with protein corona around nanoparticle, covalent coupling can occur in one monolayer at maximum, but is often less due to chemical coupling inefficiencies.[19] In addition, the available QD-based nanocarriers lack versatility and tunability. To address these issues, we chose artificial polypeptides with coiled-coil domains as one component to form a hybrid nanogel. Artificial polypeptides are readily available through biosynthetic methods. The flexibility of recombinant DNA technology allows preparation of polypeptides with precise structure at the molecular level. Sequences of interest, such as binding domains and enzyme cleavage sites can be incorporated into engineered polypeptides. Engineered polypeptides with precise structures can be used to tune the properties of the QD-based hybrid nanocarriers, such as size, surface potential, binding, and loading capacity. In addition, the nanocarriers are expected to have low cytotoxicity as their degradation products are naturally occurring amino acids.

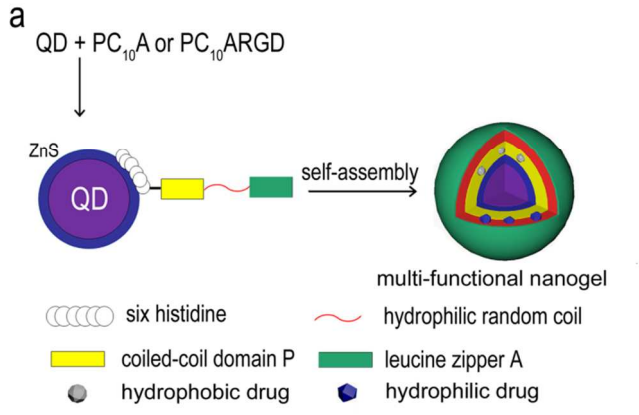

b Amino acid sequences of $PC_{10}A$ and $PC_{10}ARGD$

$PC_{10}A$: MRGS**[6H]**GSGDL**[P]**GTSYRDPMG**[C_{10}]**ARMPT**[A]**IG DHVAPRDTSW

$PC_{10}ARGD$: MRGS**[6H]**GSGDL**[P]**GTSYRDPMG**[C_{10}]**ARMPT**[A]**IG DHVAPRDTSYAVTG**RGD**SPASSTSW

Abbreviations for peptide domains:

[6H]: HHHHHH

[P]: APQMLRELQETNAALQDVRELLRQQVKEITFLKNTVMESDAS

[A]: SGDLENEVAQLEREVRSLEDEAAELEQKVSRLKNEIEDLKAE

[C_{10}]: $[AGAGAGPEG]_{10}$ (hydrophilic random coil)

Scheme 1. Schematic illustration of formation of QD-polypeptide nanogel (a), and the sequences of the polypeptides used in the study (b).

Herein, we report a new type of multi-functional QD-polypeptide hybrid nanogel which combines the capability of targeted tumor imaging with drug delivery. Coiled-coil polypeptide ($PC_{10}A$ or $PC_{10}ARGD$), which consists of an associative domain P, a zipper domain A, and a random coil midblock (C_{10}), was chosen to modify the surface of QDs by specific metal-affinity interaction between polypeptides appended with N-terminal polyhistidine sequences and hydrophilic CdSe-ZnS core-shell QDs.[20] Rigid $PC_{10}A$ or $PC_{10}ARGD$ on the surface of QDs forms a sandwich hydrogel which consists of two hydrophobic layers (formed by P domain and A domain) and one hydrophilic layer (formed by C_{10} domain) between them by self-assembly (Scheme 1). The sequences of the designed polypeptides were shown in Scheme 1. In addition, hydrophobic and hydrophilic drugs were simultaneously loaded in QD-polypeptide nanogels. These QD-polypeptide nanogels are sensitive to temperature and pH. Finally, we evaluate the binding and uptake of drug-loaded QD-$PC_{10}ARGD$ nanogel in HeLa cells which over express $\alpha_v\beta_3$ integrin receptors for simultaneous imaging and targeted delivery of drugs. The integration of these functionalities makes these QD-polypeptide nanogels as a potentially viable tool for cancer diagnosis, imaging, and therapy.

Results and discussion

Formation and characterization of the QD-polypeptide hybrid nanogel. The polypeptides immobilized on the surface of QDs have a few unique features including inherent tunability and biocompatibility to the QDs. The genetically engineered polypeptides ($PC_{10}A$, $PC_{10}ARGD$, and P) were expressed in *E. coli*, purified, and analyzed by matrix-assisted laser desorption/ionization (MALDI) mass spectrometry and SDS-polyacrylamide gel electrophoresis (SDS-PAGE) (Fig. S1). The QD-polypeptide hybrid nanogels were prepared by metal-affinity driven self-assembly between His-tagged polypeptides and CdSe-ZnS QDs. Six histidine sequences were fused into N-terminus of polypeptides to bind QDs according to previously developed method.[21] Furthermore, previous studies indicated that the number of histidine monomers beyond six does not improve polypeptide binding to ZnS capped QDs.[20] To investigate the saturation ratio of $PC_{10}A$ and QDs, hybrid QD-polypeptide of different ratios were chromatographed by capillary electrophoresis (CE) (Fig. 1a). Our previous studies showed that CE is an effective method to monitor QD-polypeptide interaction because of its superior capability in revealing subtle structural and compositional changes of surface-bound ligands on QDs.[22] As shown in Fig. 1a, the migration times of hybrid QD-polypeptide nanogels are shorter than that of the original QDs, which are probably due to the increased size of hybrid QD-polypeptide. With increasing molar ratio of polypeptide to QDs, the migration time decreases. When $PC_{10}A$:QDs ratio reaches 25:1, only a single peak with migration time of 293 s was observed in the CE, indicating that QD-$PC_{10}A$ assembly reaches saturation and form unified QD-$(PC_{10}A)_{25}$ species. The saturation ratio of $PC_{10}A$ to QD is consistent with the reported saturation ratio of monomeric proteins.[23] CE results demonstrate that QDs can be assembled with coiled-coil polypeptides by specific metal-affinity interactions, and the polypeptide on the surface of QDs can be quantified. P and $PC_{10}ARGD$ were assembled on the surface of QDs with the same procedure.

To further investigate the existing form of the polypeptide on the surface of QDs, the size and zeta potential of QDs and hybrid QD-polypeptides were measured. Dynamic light scattering (DLS) measurements and transmission electron microscopy (TEM) revealed that the size of glutathione (GSH)-coated CdSe-ZnS QDs to be 7.2 ± 0.5 nm, and they are fairly mono-dispersed (Fig. 1b and Fig. S1). The sizes of QD-P, QD-$PC_{10}A$, and QD-$PC_{10}ARGD$ complexes determined by DLS were found to be 23 ± 1, 38.2 ± 1.5, and 40.2 ± 1.2 nm, respectively, and are fairly mono-dispersed. The hydrodynamic diameters of GSH-capped QDs and QD-P measured by DLS increased from 7.2 ± 0.5 nm to 23 ± 1 nm, and the increased size corresponds to the doubled size of polypeptides P (one polypeptide P with ca. 7 nm long). On the other hand, the coiled-coil polypeptide P forms parallel pentameric aggregates exclusively.[24] These results suggest that a polypeptide monolayer self-assembles on the surface of QDs, and physically cross-linked hydrogel microstructures form through association of coiled-coil P domain.

The diameter of QD-$PC_{10}A$ increases by 15 nm relative to QD-P, indicating that a hydrophilic layer formed from C_{10} domain and a thin hydrophobic layer formed from A domain. The outside hydrophobic layer is likely to be thin because leucine zipper A domain adopts an antiparallel orientation. In addition, coiled-coil domains A and P do not associate with each other.[25] Thus, surface-bound $PC_{10}A$ ligand on QDs form a sandwich hydrogel microstructure consisting of two hydrophobic layers (formed by P domain and A domain) and one hydrophilic layer (formed by C_{10} domain) between them (Scheme 1). To promote selective cellular uptake and imaging specificity, an integrin-targeted RGD domain was successfully incorporated into the C-terminus of the polypeptide $PC_{10}A$. Nanogel formation did not change QDs core size and nanogel was mono-disperse containing one QD by the unstained TEM measurement (Fig. S2).

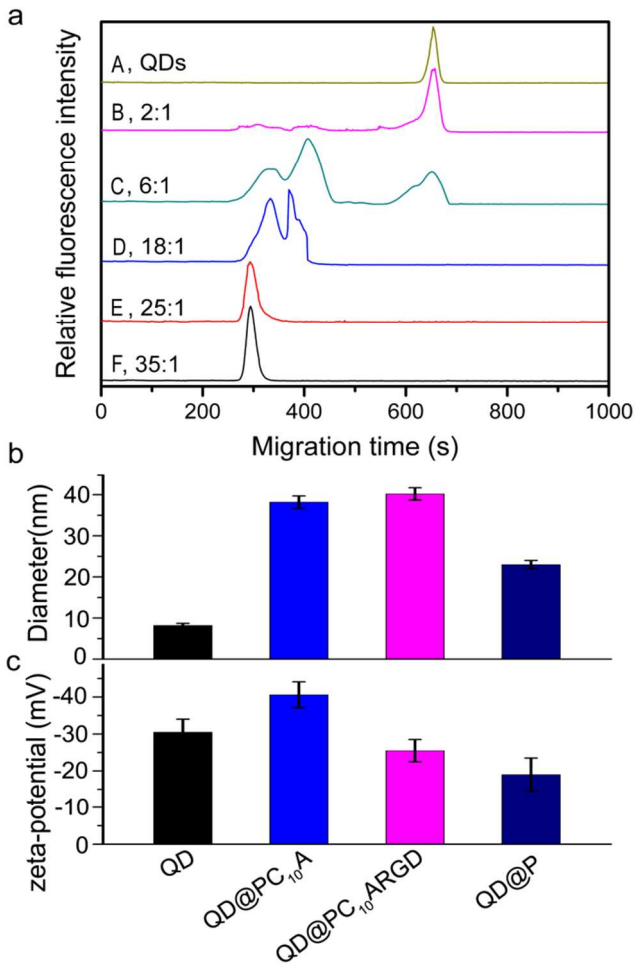

Fig. 1 Characterizations of QD-polypeptide nanogels. (a) electropherograms for the assembly of $PC_{10}A$ and GSH-capped QDs at different molar ratios, A, QDs; B, 2:1; C, 6:1; D, 18:1, E, 25:1, F, 35:1. Coated capillary with 36 cm effective (60 cm total) length and 75 μm I.D. was used. 25 mM $Na_2B_4O_7$ (pH 9.2) was used as running buffer. Applied voltage was 18 kV, and hydrodynamic injection was carried out by siphoning at 13 cm height for 20 s. λ_{ex} = 420 nm; (b) hydrodynamic diameters of QDs and QD-polypeptide nanogels measured by means of DLS; (c) zeta-potential. Error bars based on standard error of triplicates.

Zeta potential measurements show that QDs and three hybrid nanogels are highly negatively charged (Fig. 1c). The negative value is expected due to the presence of glutamic acid and aspartic acid residues of polypeptides. The zeta potential of QD-$PC_{10}A$ is lower than that of the original QDs and QD-P, most likely caused by larger number of negative residues on the C_{10} domain. While, the zeta potential of the QD-PC_{10}ARGD nanogel (-29.5 mV) is larger than that of QD-$PC_{10}A$ nanogel (-40.6 mV) because of the positive RGD sequences. Thus, the hybrid QD-polypeptide assembly system facilitated making nanoparticle with different zeta potential through tailoring the RGD ligand density. QD-polypeptide nanogels are stable in PBS at 4 ºC for at least one month.

Hybrid QD-polypeptide nanogel is highly tunable By incorporating ligands of interest into polypeptide molecules we are able to tune the physical properties of QD-polypeptide including size, shape, binding domain, and surface potential. The flexibility of recombinant DNA technology allows systematic investigation of structure-property relationships. For example, the modular design of our engineered polypeptide facilitates the creation of identical $PC_{10}A$ that differ only in the bioactive RGD ligand number.[26, 27] By designing different number of integrin-targeted RGD ligands into each $PC_{10}A$ and by maintaining a constant polypeptide concentration on the surface of QDs we can tune the density of integrin-targeted RGD ligand with similar hydrogel microstructure. The ability to control the density of active RGD ligand, and thus to study their effects on cell uptake, has been proven to be a useful strategy for understanding specific integrin-mediated interaction.[28]

Fig. 2 shows the absorption and fluorescence spectra of original QDs along with hybrid QD-polypeptide nanogels dispersed in PBS buffer. The hybrid QD-polypeptide nanogels retain the spectroscopic properties of the original nanocrystals with respect to UV-vis absorption. While, the emission peaks of QD-$PC_{10}A$ and QD-PC_{10}ARGD are found to have slight red-shifts (2 nm for QD-$PC_{10}A$ and 3 nm for QD-PC_{10}ARGD) compared with the original QDs, which might be due to increase of QDs' size after polypeptide modification. The data also show that the fluorescence intensity of hybrid QD-$PC_{10}A$ and QD-PC_{10}ARGD weaken in comparison with that of original QDs. The photoluminescence quantum yield changed from 28.7% for original QD to 25.8% for QD-$PC_{10}A$ and 27.2 % for QD-PC_{10}ARGD, respectively, which is probably due to the different zeta potential and ligand type.

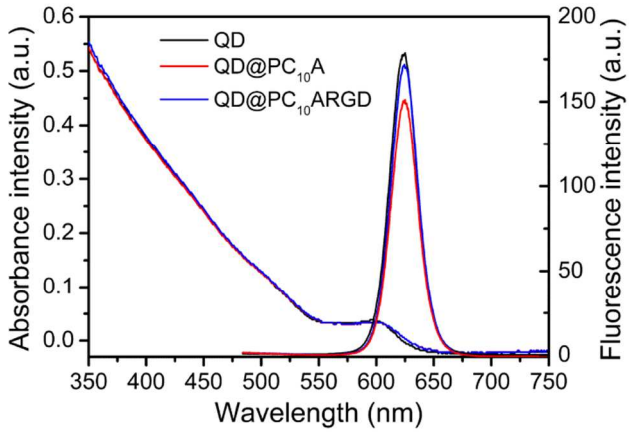

Fig. 2 The absorption spectra and fluorescence spectra of QDs, QD-$PC_{10}A$, and QD-PC_{10}ARGD.

Loading of hybrid nanogel with drugs. The integration of hydrophobic and hydrophilic drugs in a nanogel offers the chance to develop a new drug delivery system that combines the best features of these two distinct classes of drugs. Hydrophobic or hydrophilic molecules can be loaded in the hydrophobic or hydrophilic domain present in some nanogels.[29] Therefore, hydrophobic and hydrophilic drugs are expected to encapsulate simultaneously into the QD-PC_{10}A and QD-PC_{10}ARGD hybrid nanogels. As proof of principle that hybrid nanogels could potentially be used as nanocarriers for hydrophobic and hydrophilic drugs, we loaded them with hydrophobic dye (2-amino-4,6-bis-[(4-N,N'-diphenylamino)styryl] pyrimidine, ABDPSP)[30] and hydrophilic dye (fluorescein sodium), which are used here as model drugs. Sequential assembly approach was used to load hydrophobic and hydrophilic cargoes, which involved forming the hybrid nanogel first, then adding payload. The loading of hydrophilic drug or hydrophobic drug was followed by agarose gel electrophoresis and the fluorescence spectra of separated products were collected on an inverted fluorescence microscope equipped with a fiber optic spectrometer (Fig. 3a). All samples migrate towards the positive electrode because of negative charges on their surfaces. When QDs were modified with polypeptide, the conjugates migrated more slowly through gels than QDs alone due to the retarded electrophoretic mobility. The QD-polypeptide (lane 2) does not show tailing on the gel, further indicating that QD-PC_{10}ARGD assembly reaches saturation and form a single species

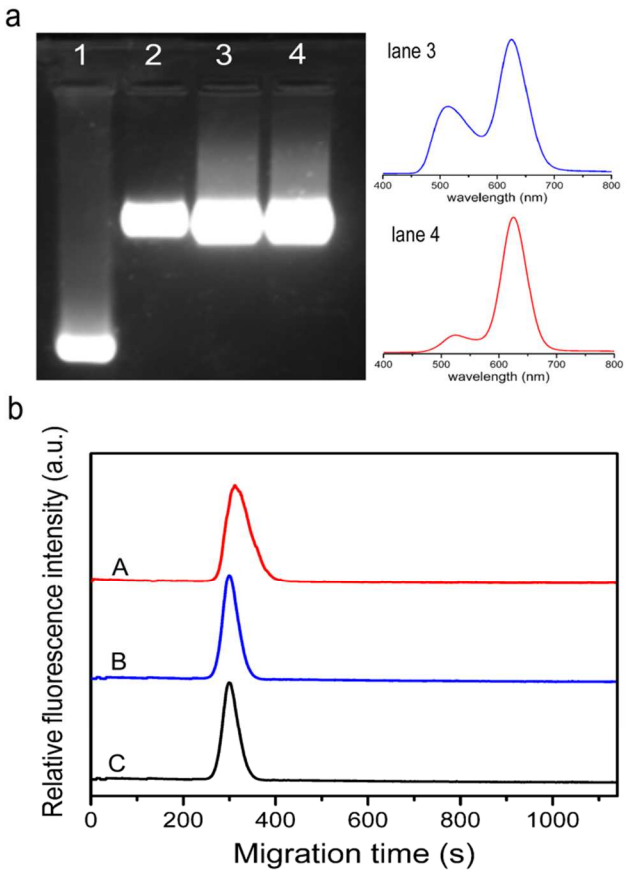

Fig. 3 Loading QD-polypeptide with hydrophobic and hydrophilic drugs. (a) agarose gel electrophoresis (left) of GSH-capped QDs (lane 1), QD-PC_{10}ARGD (lane 2), QD-PC_{10}ARGD-ABDPSP (lane 3), and QD-PC_{10}ARGD-fluorescein sodium (lane 4), and fluorescence spectra (right) of lane 3 and lane 4. λ_{ex} = 420 nm; (b) electropherograms of QD-PC_{10}ARGD (curve A), QD-PC_{10}ARGD-ABDPSP (curve B), and QD-PC_{10}ARGD-fluorescein sodium (curve C). Other conditions were same as described in Fig. 1.

which is consistent with the result of CE. Loaded QD-PC_{10}ARGD with hydrophobic dye or hydrophilic dye (lane 3 and 4) did not show any retardation of the bands. The fluorescence spectra of QD-PC_{10}ARGD-ABDPSP and QD-PC_{10}ARGD-fluorescein sodium bands were also shown in Fig. 3a. Two emission peaks were observed in each fluorescence spectra, and these peaks were easily identified to be the QD-PC_{10}ARGD and loaded dyes according to its characteristic wavelength.[30] This result suggests that hydrophilic and hydrophobic drugs were loaded successfully in QD-PC_{10}ARGD nanogel. Previous studies have shown that coiled-coil P domain assembles into a pentameric cylinder-like and hydrophobic core that is 7.3 nm long with a diameter of 0.2-0.6 nm, and it can specifically load some hydrophobic drugs, such as vitamin D_3, trans retinol (ATR) and curcumin (CCM).[24] Therefore, drugs loading in QD-PC_{10}A and QD-PC_{10}ARGD would be universal in drug delivery.

To further confirm the presence of hydrophobic dye in QD-PC_{10}ARGD, hybrid nanogel with loaded drug was analyzed by CE (Fig. 3b). In our CE experiments, two signal channels of fiber optic spectrometer with fixed detecting wavelength at 500 ± 10 and 620 ± 10 nm were used to simultaneously collect the fluorescence signal of QD-PC_{10}ARGD and encapsulated dye. Experimental results proved that there was no cross-talk between the QD-PC_{10}ARGD and dye channel (Fig. S3). One electrophoresis peak, with slight short migration time compared with that of hybrid QD-PC_{10}ARGD nanogel (Fig. 3, curve A), was observed in the QD-PC_{10}ARGD channel (Fig. 3, curve B), indicating that the electric charge of hybrid nanogel with and without loaded drug is slightly different. In the dye channel, only one electrophoresis peak (Fig. 3, curve C) whose corresponding migration time was the same as that of peak obtained in the QD-PC_{10}ARGD channel was observed, and it should correspond to the loaded dye in the hybrid nanogel.

Drug release of QD-polypeptide nanogel system in vitro. Coiled-coil polypeptides usually undergo diverse conformational transitions in response to temperature, pH, ionic strength, and solvent and so forth.[31] Since the hydrophobic drug was loaded in the hydrophobic layers formed by coiled-coil P domain and A domain, it is expected to show thermal-responsive and pH-responsive drug release.[25, 31] To demonstrate this, time-dependent release of hydrophobic dye from the hybrid nanogel were carried out in a two-phase dichloromethane (DCM)-water system at different temperature as previously described.[32] As shown in Fig. 4a, a rapid increase in fluorescence intensity was observed along with transfer of dye into the DCM layer, and reached to a constant value. No QD-QD-PC_{10}A nanogels were observed in the DCM layer, indicating that the drug release occurs interfacially. In addition, with increasing temperature, the release rate and release amount of the dye increased gradually. The drug release amount at 37 ºC is seven times the amount released at 25 ºC, and the release amount further reaches twelve times at 60 ºC. These observations indicate that the QD-polypeptide is thermal-responsive. The release rate and release amount did not increase when the temperature above 60 ºC (data not shown). This is probably due to the relatively low melting temperature (*Tm*) of P domain (about 41 ºC).[24]

To further investigate whether these hybrid nanogels show pH-responsive drug release, the release kinetics of the encapsulated hydrophobic dye from hybrid nanogel was measured in the two-phase DCM-water system at different pH values. As shown in Fig.

4B, release amounts of hydrophobic dye from the QD-$PC_{10}A$ nanogel at pH 7.4 were slightly higher than that of pH 6. However, the cumulative release amounts of hydrophobic dye at pH 10 or pH 4.5 were more than twice the amount at pH 6, which is probably due to the conformational transitions of P domain and A domain when the pH deviated largely from physiological pH. These results corroborate the claim that the QD-Polypeptide nanogels are pH sensitive. The change of release amount in pH from 7.4 to 4.5 will be definitely beneficial to effective cancer treatment.[33]

Exchanging the bound ligands on the surface of nanoparticles often provides a method to release the encapsulated drugs on the ligands.[21, 34] We utilized the competitor imidazole to displace the polypeptide on the surface of QDs, and monitored ligand displacement by CE. The saturated hybrid nanogel was prepared by mixing polypeptide and QDs with a ratio of 25:1 and purified over Sephadex 100 media to remove the unconjugated polypeptide. The saturated QD-$PC_{10}A$ nanogel has a single peak with the migration time of 293 s. Imidazole was added to the hybrid nanogel to a final concentration of 1 mM and was detected by CE at different time intervals of mixing (Fig. 4c). Two new peaks in CE with retention time of around 400 s were observed after incubation for 2 min and 5 min, indicating that a certain percentage of surface ligands on the QDs were displaced with imidazole to form QD-$(PC_{10}A)_m$-$(imidazole)_n$ (m < 25, m unknown). The peak intensity of QD-$(PC_{10}A)_{25}$ decreased gradually, and the peak intensity of QD-$(PC_{10}A)_m$-$(imidazole)_n$ increased over time. This suggests that the displacement step is time-dependent. In addition, the displacement intermediates at different time intervals (2 min and 5 min) with identical migration times were observed, indicating that displacement ratio is constant in a certain concentration of imidazole. As described in the previous report, the percentage of displacement with imidazole is dependent on the concentration of imidazole (Fig. S4).[21] Interestingly, the re-binding step was observed after the displacement step. After adding imidazole for 15 min, the intermediates QD-$(PC_{10}A)_m$-$(imidazole)_n$ were replaced with QD-$(PC_{10}A)_{25}$ nanogel.

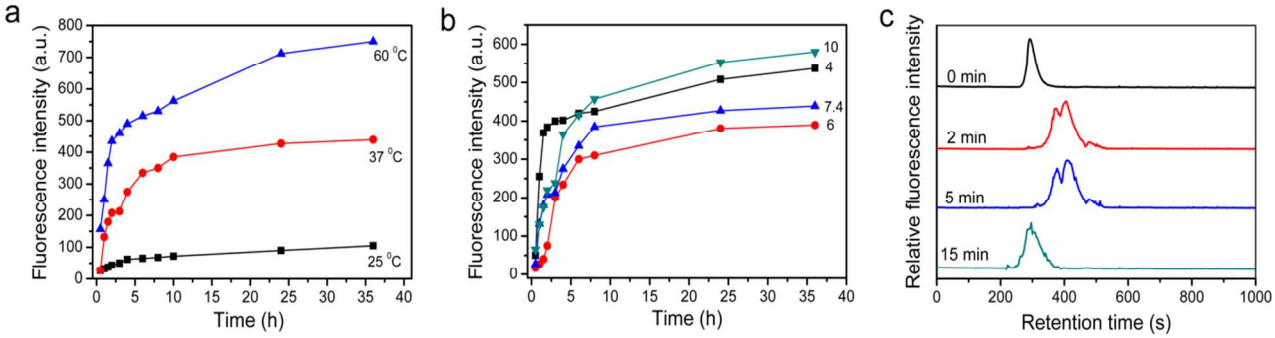

Fig. 4 *In vitro* release of hydrophobic drug from the QD-$PC_{10}A$ nanogel. (a) time-dependent release in DCM-aqueous solution two-phase systems (λ_{ex} = 430 nm, pH = 7.4) at different temperatures (25 ºC, 37 ºC, and 60 ºC); (b) time-dependent release in DCM-aqueous solution two-phase systems (λ_{ex} = 430 nm, 37 ºC) at different pH (4, 6, 7.4, 10); (c) electropherograms of displacement by 1 mM imidazole at different time points. Other conditions were same as described in Fig. 1.

Targeted imaging and drug delivery in vitro. For the effective drug delivery and imaging, it is desirable that the drug-loaded hybrid nanogel can enter the target cell. As many effective drugs are hydrophobic, such as PDT agents, we chose to investigate the delivery of hydrophobic drugs to a target remains. RGD tripeptide was chosen to selectively bind integrin $\alpha_v\beta_3$ in cell culture on various cell lines. To evaluate the integrin $\alpha_v\beta_3$ binding affinity of hybrid nanogel *in vitro*, we chose human cervical carcinoma HeLa cells (high integrin $\alpha_v\beta_3$ expression) for target-specific imaging, and the human breast cancer cell line MCF-7 (low integrin $\alpha_v\beta_3$ expression) as the control.[35] The cells were incubated with hybrid nanogel for 2 h at 37 ºC, and examined under a confocal laser scanning microscope. The representative brightfield and fluorescence images are shown in Fig. 5.

It can be seen clearly that strong green dye signal and red QDs signal were observed within the integrin-positive HeLa cells after incubation with QD-PC_{10}ARGD-ABDPSP nanogel, whereas cell incubation with QD-PC_{10}A-ABDPSP nanogel showed much less fluorescence. This result indicates that the binding and delivery are mainly contributed to RGD tripeptide on the surface of QDs. In contrast, integrin-negative cell controls (MCF-7) incubation with QD-PC10ARGD-ABDPSP nanogel showed very weak green and red signals. This result suggests that hydrophobic drug is able to deliver into cells by hybrid nanogel uptake. Compared with QD-PC10A nanogel, cell incubation with GSH-capped QDs showed stronger fluorescence (Fig. S5). Lower non-specific binding of QD-$PC_{10}A$ nanogel is expected to reduce background and improve signal-to-noise ratio in imaging. Targeted QD-PC_{10}ARGD nanogel with lower non-specific binding is expected to prolong its circulation time in the bloodstream and result in highly selective accumulation at the targeting site. Integrin receptor specificity of QD-PC_{10}ARGD was further demonstrated by a competition assay. The HeLa cells were pre-incubated with a 500-fold molar excess of PC_{10}ARGD polypeptide at 37 ºC for 1 h and incubated with QD-PC_{10}ARGD-ABDPSP nanogel at 37 ºC for another 2 h. Only very weak green and red fluorescence were observed. These results demonstrate that multi-functional drug-loaded QD-PC_{10}ARGD nanogel achieved simultaneously targeted imaging and drug delivery *in vitro*.

Additionally, flow cytometry was used to determine the integrin binding capability of the hybrid QD-PC_{10}ARGD nanogel. Fig. 6 shows the fluorescence intensities of flow cytometry after the integrin-positive HeLa cells and the integrin-negative MCF-7 cells were incubated with the hybrid nanogels for 2 h. When the QD-PC_{10}ARGD nanogel was used in HeLa cells, the mean fluorescence intensity was much higher than that of the QD-$PC_{10}A$ nanogel and pre-incubated PC_{10}ARGD polypeptide. This suggests more binding or uptake of the QD-PC_{10}ARGD nanogel to the HeLa cells. In contrast, very low mean fluorescence intensities of integrin-negative MCF-7 cells incubated with all hybrid nanogels were observed, confirming that the HeLa cells express a higher amount of $\alpha_v\beta_3$

integrin than the MCF-7 cells. Thus, the results of flow cytometry studies are consistent with the result of the confocal fluorescence microscopy imaging (Fig. 5).

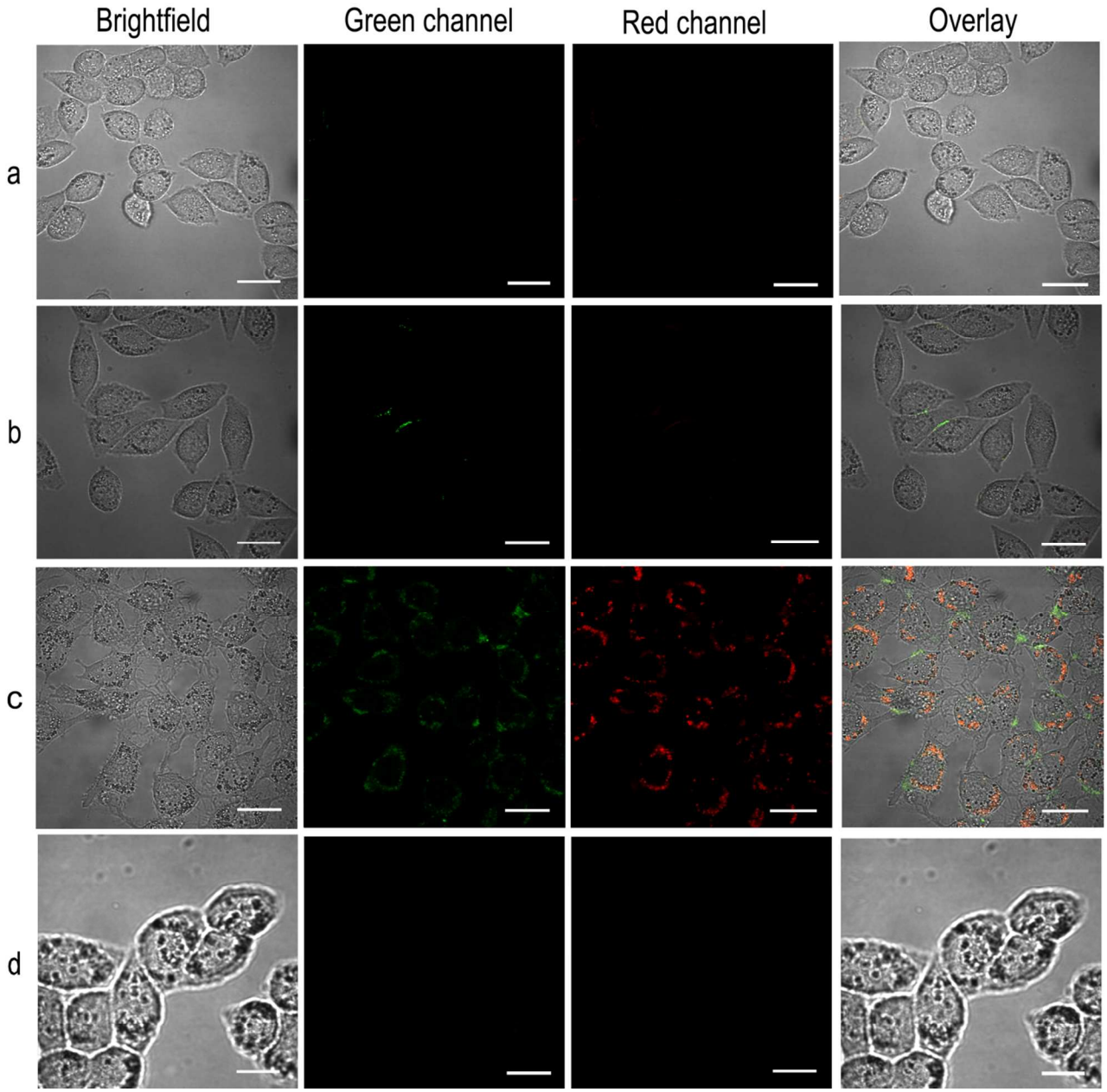

Fig. 5 Confocal fluorescence images of (a) HeLa cells incubated with 2 nM QD-PC_{10}A-ABDPSP nanogel, (b) HeLa cells pre-incubated with 1 μM PC_{10}ARGD for 1 h before the addition of 2 nM QD-PC_{10}ARGD-ABDPSP nanogel, (c) HeLa cells incubated with 2 nM QD-PC_{10}ARGD-ABDPSP nanogel, (d) MCF-7 cells incubated with 2 nM QD-PC_{10}ARGD-ABDPSP nanogel. The green and red channel was collected at 500 ± 10 nm and 620 ± 10 nm, respectively. A 100× oil-immersion objective (1.40 numerical apertures) was used. Scale bars are 20 μm.

***In vitro* cytotoxicity.** QDs are considered intrinsically harmful because divalent cations and heavy metals in their structures can cause acute and chronic toxicities. Surface coatings that limit the leakage of heavy metal ions can reduce the potential toxicity of QDs. Studies show that the thickness and stability of QDs surface coating are the major factors of QDs cytotoxicity.[36] To evaluate the cytotoxicity of the hybrid nanogels, a MTT [3-(4,5-di-methylthiazol-2-yl)-2,5-diphenyltetrazolium bromide] assay with the HeLa cancer cells and NIH 3T3 normal cells was used to determine the effect of hybrid nanogels on cell proliferation after 24 h.

Fig. 7a shows a comparison of the *in vitro* HeLa cell viability of free PC_{10}ARGD polypeptide, GSH-capped QDs, and QD-PC_{10}ARGD nanogel at different concentration after 24 h culture. For HeLa cancer cells, the cell viabilities at different concentrations for free PC_{10}ARGD polypeptide are almost 100%, suggesting that PC_{10}ARGD polypeptide is nontoxic. In addition, the cell viability for

GSH-capped QDs is lower compared to the QD-PC_{10}ARGD nanogel at different concentration as shown in Fig. 8a. The cell viability for the QD-PC_{10}ARGD nanogel is 99 ± 6.2%, 97 ± 7.2%, and 94 ± 7.5% at 10 nM, 50 nM, and 100 nM, respectively. These are higher than the cell viability for GSH-capped QDs which is 87 ± 5.7%, 85 ± 8.2%, and 81 ± 6.1% at 10 nM, 50 nM, and 100 nM, respectively. The cell viability for GSH-capped QDs is higher than that for QDs functionalized with organic ligands.[37] It is probable that GSH is a short peptide. With increasing probe concentration, the cell viabilities slightly decrease. This indicates that the QDs coated with polypeptide hydrogen decreased the cytotoxicity of the QDs. This may be attributed to nanogel formation by the nontoxic polypeptide and the targeting effects of RGD, which is consistent with earlier observations that the increased uptake of modified QDs into the cancer cells through the receptor-mediated endocytosis caused the decrease in cell viability.[38]

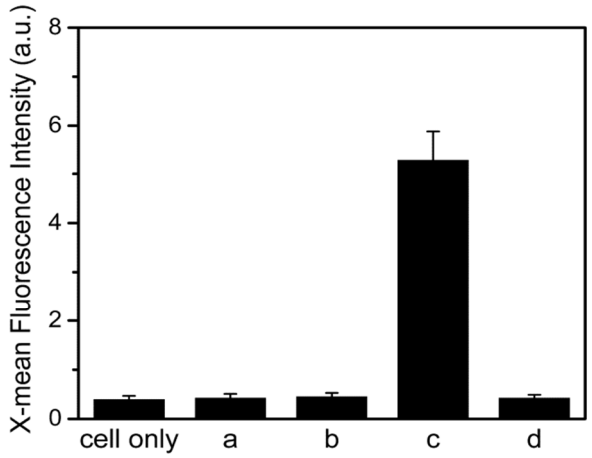

Fig. 6 Flow cytometry of (a) HeLa cells incubated with 2 nM QD-PC_{10}A nanogel, (b) HeLa cells pre-incubated with 1 μM PC_{10}ARGD for 1 h before the addition of 2 nM QD-PC_{10}ARGD nanogel, (c) HeLa cells incubated with 2 nM QD-PC_{10}ARGD nanogel, (d) MCF-7 cells incubated with 2 nM QD-PC_{10}ARGD nanogel.

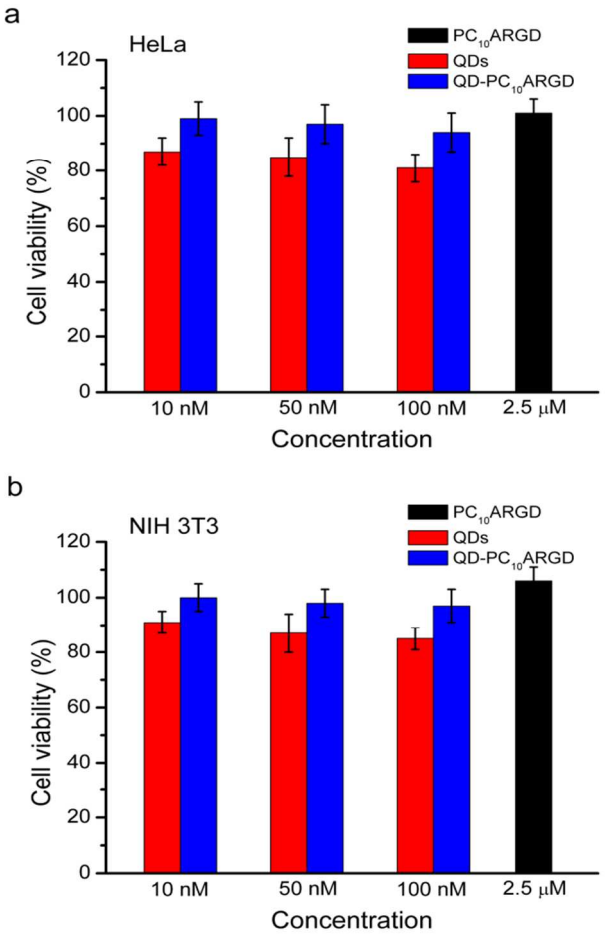

Fig. 7 *In vitro* viability of HeLa cells (a) and NIH 3T3 cells (b) treated with free PC_{10}ARGD polypeptide, GSH-capped QDs, and QD-PC_{10}ARGD nanogel at different concentration. The concentration of free PC_{10}ARGD polypeptide is 2.5 μM, and the concentrations of GSH-capped QDs and QD-PC_{10}ARGD nanogel are 10 nM, 50 nM, and 100 nM.

Fig. 7b shows a comparison of the *in vitro* NIH 3T3 cell viability of free PC_{10}ARGD polypeptide, GSH-capped QDs, and QD-PC_{10}ARGD nanogel at different concentration after 24 h culture. We used free PC_{10}ARGD polypeptide, without QDs, and verified that it also produced low cell viability for NIH 3T3 cells as shown in Fig. 7b. The cell viability for the QD-PC_{10}ARGD nanogel is 100 ± 5.2%, 98 ± 5.1%, and 97 ± 6.1% at 10 nM, 50 nM, and 100 nM, respectively. While the cell viability for GSH-capped QDs is 91 ± 4.3%, 87 ± 8.1%, and 85 ± 4.7% at 10 nM, 50 nM, and 100 nM, respectively. Therefore, the *in vitro* cell viability experiments showed that the QD-PC_{10}ARGD nanogel has less cytotoxicity than free QDs for NIH 3T3 fibroblasts normal cells. This is very important because the hybrid nanogels are used for imaging and delivery purposes and should not damage the surrounding normal cells. The NIH 3T3 cell viability experiments demonstrated that the QDs coated with polypeptide hydrogen decreased the cytotoxicity of QDs for normal cells.

Conclusions

A new type of multi-functional QD-polypeptide hybrid nanogel that combines the capability of targeted tumor imaging with drug delivery were designed and prepared. We demonstrated that surface ligands consisting self-assembly of coiled-coil domains on the QD-PC_{10}A and QD-PC_{10}ARGD nanogels can form the sandwich microstructure by CE and DLS measurement. We are able to tune the physical properties of QD-polypeptide including size, shape, binding domain, and surface potential. The successfully simultaneous loading of hydrophobic and hydrophilic drugs into the hydrophobic and hydrophilic layer of QD-PC_{10}A or QD-PC_{10}ARGD nanogel demonstrated their potential for drug delivery applications. QD-polypeptide will provide a general avenue for the fabrication of dual drug vehicular nanocarriers. Temperature- and pH-sensitive polypeptide monolayer on the QDs can serve as a trigger to control the release of the loaded hydrophobic cargo. Uptake of drug-loaded QD-PC_{10}ARGD nanogel in $\alpha_v\beta_3$ overexpressing cells was remarkably greater than in control cells, and the QD-PC_{10}A revealed lower non-specific binding than GSH-capped QDs. Compared with the original QDs, the QD-polypeptide nanogels showed lower *in vitro* cytotoxicity for both HeLa cells and NIH 3T3 cells. Furthermore, cytotoxicity of targeted QD-polypeptide nanogel is lower for normal NIH 3T3 cells than that for HeLa cancer cells. The results reported here open up new perspectives for targeting imaging and drug delivery.

Experimental section

Materials. Cadmium acetate ($Cd(Ac)_2$), zinc acetate ($Zn(Ac)_2$), and selenium (Se) were obtained from Acros Organics. Restriction endonuclease NheI, SpeI, and T4 DNA ligase were obtained from New England Biolabs Inc. (Beijing, China). Ni-NTA separation column was purchased from Qiagen China (Shanghai) Co., Ltd. Ultrapure water (≥18.2 MΩ) purified by Milli-Q system (Millipore, USA) was used for preparation of all solutions. All other reagents were purchased from Sigma-Aldrich, Inc. (St. Louis, MO) unless otherwise specified.

Synthesis and purification of the polypeptide. $PQE9PC_{10}A$ plasmid was a gift from Prof. David Tirrell at the California Institute of Technology Pasadena, CA. The segment encoding RGD and containing NheI and SpeI restriction sites was synthesized by the method of polymerase chain reaction (PCR). The RGD segment was digested by NheI and SpeI, and the $PQE9PC_{10}A$ plasmid was digested by SpeI to yield cohesive ends. Digested RGD and $PQE9PC_{10}A$ were ligated with T4 DNA ligase to construct $PQE9PC_{10}ARGD$ plasmid. PQE9P plasmid was constructed through the similar method. The sequences of PQE9P, $PQE9PC_{10}A$, and $PQE9PC_{10}ARGD$ were verified at the DNA sequencing core facility of Sunny Institute at Shanghai. PQE9P, $PQE9PC_{10}A$, and $PQE9PC_{10}ARGD$ plasmids were transformed into *E. coli* strain M15, respectively. Bacterial culture was grown at 37 ºC in 1 L of 2xYT media supplemented with 50 mg/L of ampicillin and 25 mg/L of kanamycin. The culture was induced with 1 mM isopropyl-β-D-thiogalactoside (IPTG) when the optical density at 600 nm reached 0.7-1.0. The culture was continued for an additional 4 h. Cells were harvested by centrifugation (6,000 g, 30 min) and lysed in 8 M urea (pH = 8.0). The cell lysate was centrifuged at 12,000 g for 30 min, and the supernatant was collected for purification. A 6×Histidine tag encoded in pQE9 vector allows the polypeptide to be purified by affinity chromatography on a Ni-NTA resin following the denaturing protocol provided by Qiagen. The eluted fractions were dialyzed against sterile water for three days at room temperature, frozen, and lyophilized. The purified polypeptides were characterized using a Bruker Reflex III reflectron MALDI-TOF mass spectrometer and 12% SDS-PAGE. $PC_{10}A$ (MS: 20861.4 Da, the theoretical calculation of molecular weight: 20858.5 Da), $PC_{10}ARGD$ (MS: 22210.7 Da, the theoretical calculation of molecular weight: 22295.9 Da), P (MS: 8399.1 Da, the theoretical calculation of molecular weight: 8395.2 Da).

Preparation of CdSe-ZnS core-shell QDs. Oil-soluble core-shell QDs (CdSe-ZnS) were synthesized according to the literature method developed by our lab.[39] Different-sized oil-soluble QDs with different emission wavelengths were obtained by controlling the temperature and initial molar ratio of reactants.

Water-soluble QDs was prepared by a surface ligand exchange reaction between TOPO and the hydrophilic substance. In brief, 0.2 g GSH was added to 1 mL CdSe-ZnS chloroform solution in a centrifuge tube under vigorous stirring. After stirring for 12 h, 100 μL 1 M NaOH and 400 μL ultrapure water were added to the mixture. Mixture was precipitated by acetone. After centrifugation (6,000 g, 10 min), the precipitate was washed by acetone and redispersed in 500 μL PBS (0.01 M, pH 7.4). The concentrations of QDs solutions were calculated by an equation proposed by Peng's group,[40] and the photoluminescence quantum yields of QDs were measured by an optically dilute method using rhodamine 6G as reference standard.[41] QDs size was determined by a Tecnai G^2 20 U-Twin TEM.

Procedure of CE. CE analyses were carried out on a home-built system according to our previous work.[22] Briefly, a 75 μm inside diameter (I.D.) × 365 μm outside diameter (O.D.) fused-silica capillary was fixed on the stage of an inverted fluorescence microscope (IX71, Olympus, Japan), and a detection window was simply made by burning a specific length of polyimide coating of capillary above the objective lens of microscope. A 100-W mercury lamp was used as an excitation light source. The fluorescence of QDs were collected by an optical system and recorded by a fiber optic spectrometer (QE65000, Ocean Optics, USA). The effective capillary length was 36 cm. Normal polarity conditions, i.e. the cathode at the capillary outlet end, hydrodynamic injection by siphoning (13 cm, 20 s) at anode, were used for all CE separations. CE analysis was achieved at room temperature. A solution of 25 mM, pH 9.2 sodium borate was used as electrophoresis separation buffer.

Preparation of the QD-polypeptide nanogels. For QD-polypeptide self-assembly, polypeptide was mixed with QDs in PBS at room temperature. Various concentrations of polypeptide were added in 0.5 μM GSH-capped QDs, and mixture was incubated for 1 h to allow the assembling to complete. QD-polypeptide was purified over Sephadex 100 media to remove unconjugated polypeptide. QD-$PC_{10}A$ nanogels with differ molar ratio of QDs and $PC_{10}A$ were analyzed by CE. The UV-vis absorption spectra of QDs and QD-polypeptide nanogels were recorded on a UV-2550 UV-vis spectrophotometer (Shimadzu, Japan). The fluorescence spectra of QDs and QD-polypeptide nanogels were measured using a LS-55 spectrophotometer (PerkinElmer, USA) at room temperature.

The hydrodynamic size and zeta potential of GSH-capped QDs, QD-P, QD-$PC_{10}A$, and QD-$PC_{10}ARGD$ were determined on a ZS90 Nanosizer (Malvern, UK) at 25 ºC by DLS and laser doppler electrophoresis methods, respectively.

Loading hydrophobic and hydrophilic drugs. Hydrophobic and hydrophilic model drugs were loaded into QD-polypeptide by using two different approaches. For loading hydrophobic drug, a hydrophobic dye ABDPSP was used as a model drug. Acetone (1 mL) and 25 μL 4 M NaOH were added in 500 μL QD-polypeptide (1 μM, molar ratio of QDs:polypeptide 1:25) in a centrifuge tube. After centrifugation (6,000 g, 10 min), the precipitate was dried with a gentle nitrogen gas stream. Then, 200 μL 2×10^{-2} M ABDPSP in dimethylsulfoxide (DMSO) was added, and mixture was stirred at room temperature for 8 h. QD-polypeptide with payload was centrifuged at 10,000 g for 10 min. Finally, the precipitate was dissolved in 500 μL PBS. For loading hydrophilic drug, a hydrophilic dye (fluorescin sodium) was used as model drug. Fluorescin sodium (10 μL, 0.2 M) was added in 500 μL QD-polypeptide (1 μM, molar ratio of QDs:polypeptide 1:25), followed by incubation at room temperature. After incubation for 2 h, the mixture was precipitated by acetone. After centrifugation (6,000 g, 10 min), the precipitate was washed by acetone and redissolved in PBS. Two precipitation/dissolution cycles were performed. Finally, the precipitate was dissolved in 500 μL PBS. GSH-capped QDs, QD-$PC_{10}ARGD$, QD-$PC_{10}ARGD$-ABDPSP, and QD-PC10ARGD-fluorescein sodium were separated by 0.8% agarose gel. 1× TAE buffer (Tris base/acetic acid) was used as the running buffer. The gel was run for 30 min at a constant voltage of 130 V and imaged on a UV transilluminator of the WD-9413A Gel Documentation & Analysis System with an excitation wavelength of 365 nm. The fluorescence spectra of separated bands were collected by the inverted fluorescence microscope equipped with the fiber optic spectrometer.

***In vitro* drug release.** Two milliliter of DCM was added in a 1 cm quartz cuvette which was placed on a magnetic stirrer. QD-PC_{10}ARGD-ABDPSP (100 μL) was centrifuged at 10,000 g for 10 min and diluted with 900 μL PBS. The diluted QD-PC_{10}ARGD-ABDPSP was added gently without disturbing the DCM layer and incubated at different temperature (25 ºC, 37 ºC, and 60 ºC). The transfer of ABDPSP into the organic phase was monitored by fluorescence spectrophotometry (LS-55 spectrophotometer). To measure pH sensitivity of drug-loaded QD-polypeptide, the diluted QD-PC_{10}ARGD-ABDPSP was adjusted to different pH (4, 6, 7.4, and 10) and measured at 37 ºC with the same procedure.

Imidazole was added in QD-PC_{10}A (0.5 μM) with a final concentration of 1 mM at room temperature and monitored by CE at different time points.

Cell imaging. For qualitative study, HeLa cells and MCF-7 cells were seeded in 35 mm glass bottom culture dishes (MatTek) in their respective medium and cultured in a cell incubator (5% CO_2, 37 ºC). After incubation for 24 h, the adherent cells were washed twice with PBS. Drug-loaded QD-polypeptide (QD-PC_{10}A-ABDPSP or QD-PC_{10}ARGD-ABDPSP) in serum-free DMEM at 2 nM were added and incubated for another 2 h. For competitive-binding experiments, the cells were preincubated with 1 μM PC_{10}ARGD for 1 h before the addition of 2 nM QD-PC_{10}ARGD-ABDPSP. The cells were further incubated at 37 ºC for 2 h. Subsequently, the cells were washed with ice-cold PBS three times and imaged immediately with a 100× oil-immersion objective on an Olympus FLUOVIEW FV1000 confocal laser scanning microscopy.

Flow cytometry analysis. For flow cytometry analysis, HeLa cells and MCF-7 cells were seeded in 6-well plates in their respective medium and cultured in a cell incubator (5% CO_2, 37 ºC). The cells were washed with PBS three times when the cells grown to about 70%-80% confluence. Drug-loaded QD-polypeptide (QD-PC_{10}A-ABDPSP or QD-PC_{10}ARGD-ABDPSP) in serum-free DMEM at 2 nM were added and incubated for 2 h. For competitive-binding experiments, the cells were preincubated with 1 μM PC_{10}ARGD for 1 h before the addition of 2 nM QD-PC_{10}ARGD-ABDPSP. The cells were further incubated at 37 ºC for another 2 h. The cells were washed twice with PBS and trypsinized using 0.05% trypsin-EDTA. Finally, cells were suspended in PBS and analyzed with a flow cytometry instrument (FC500, Beckman Coulter) equipped with a 488 nm argon laser. To quantify effects of different treatments on cellular uptake, the median of cell fluorescence distribution (X-mean) in experiment was normalized to X-mean of untreated control.

***In vitro* cytotoxicity.** HeLa cells and NIH 3T3 cells were seeded in 96-well plates (5000 cells per well). After incubation for 24 h, the medium was discarded, and the cells were incubated with a series of concentrations of GSH-capped QDs, QDs-PC_{10}ARGD (10 nM, 50 nM, and 100 nM) and PC_{10}ARGD (2.5 μM) for another 24 h. The incubated cells were assayed for cell viability with MTT. The cells were washed twice with PBS, and MTT (20 μL, 5 mg/mL) solution was added to each well. After incubation for 4 h, the medium was discarded, and the insoluble purple formazan crystals were dissolved with DMSO (150 μL). The absorbance at 490 nm was recorded with a microplate reader (BioTek ELX808IU, USA). The absorbance was directly correlated with cell quantity, and cell viability was calculated by assuming 100% viability in the control.

Acknowledgements

This work was supported by the National Key Technology R&D Program of China (2012BAI23B02), the National Natural Science Foundation of China (Grant No. 31100704, 81271616), the Foundation for Innovative Research Groups of the NNSFC (Grant No. 61121004), and the Fundamental Research Funds for the Central Universities (Hust, 2013TS085). The authors thank Prof. David Tirrell for generously providing PQE9PC_{10}A plasmid. We also thank the facility support of the Center for Nanoscale Characterization and Devices, Wuhan National Laboratory for Optoelectronics (WNLO) and Analytical and Testing Center (HUST).

Notes and references

1. Z. Cheng, A. A. Zaki, J. Z. Hui, V. R. Muzykantov and A. Tsourkas, *Science* 2012, **338**, 903.
2. V. P. Torchilin, *Adv. Drug Deliv. Rev.* 2012, **64**, 302.
3. B. Atmaja, B. H. Lui, Y. Hu, S. E. Beck, C. W. Frank and J. R. Cochran, *Adv. Funct. Mater.* 2010, **20**, 4091.
4. K. E. Sapsford, W. R. Algar, L. Berti, K. B. Gemmill, B. J. Casey, E. Oh, M. H. Stewart and I. L. Medintz, *Chem. Rev.* 2013, **113**, 1904.
5. X. Michalet, F. F. Pinaud, L. A. Bentolila, J. M. Tsay, S. Doose, J. J. Li, G. Sundaresan, A. M. Wu, S. S. Gambhir and S. Weiss, *Science* 2005, **307**, 538.
6. M. Zhang, Y. Yu, R. Yu, M. Wan, R. Zhang and Y. Zhao, *Small* 2013, **9**, 4183.
7. W. Wang, D. Cheng, F. Gong, X. Miao and X. Shuai, *Adv. Mater.* 2012, **24**, 115.
8. P. Zrazhevskiy, M. Sena and X. Gao, *Chem. Soc. Rev.* 2010, **39**, 4326.
9. R. Kikkeri, B. Lepenies, A. Adibekian, P. Laurino and P. H. Seeberger, *J. Am. Chem. Soc.* 2009, **131**, 2110.
10. A. Anas, T. Okuda, N. Kawashima, K. Nakayama, T. Itoh, M. Ishikaw and V. Biju, *ACS Nano* 2009, **3**, 2419.
11. O. Lieleg, M. Lopez-Garcia, C. Semmrich, J. Auernheimer, H. Kessler and A. R. Bausch, *Small* 2007, **3**, 1560.
12. W. Liu, M. Howarth, A. B. Greytak, Y. Zheng, D. G. Nocera, A. Y. Ting and M. G. Bawendi, *J. Am. Chem. Soc.* 2008, **130**, 1274.
13. C. Schieber, A. Bestetti, J. P. Lim, A. D. Ryan, T. Nguyen, R. Eldridge, A. R. White, P. A. Gleeson, P. S. Donnelly, S. J. Williams, P. A. Gleeson, P. S. Donnelly, S. J. Williams and P. Mulvaney, *Angew. Chem. Int. Ed.* 2012, **51**, 10523.
14. V. Biju, T. Itoh and M. Ishikawa, *Chem. Soc. Rev.* 2010, **39**, 3031.
15. S.Marrache and S. Dhar, *Proc. Natl. Acad. Sci. USA* 2013, **110**, 9445.
16. M. J. Sailor and J. Park, *Adv. Mater.* 2012, **24**, 3779.
17. B. Zhang, Y. Zhang, S. K. Mallapragada and A. R. Clapp, *ACS Nano* 2011, **5**, 129.
18. A. Aime, N. Beztsinna, A. Patwa, A. Pokolenko, I. Bestel and P. Barthelemy, *Bioconjugate Chem.* 2013, **24**, 1345.
19. J. C. Y. Kah, J. Chen, A. Zubieta and K. Hamad-Schifferli, *ACS Nano* 2012, **6**, 6730.
20. K. E. Sapsford, T. Pons, I. L. Medintz, S. Higashiya, F. M. Brunel, P. E. Dawson and H. Mattoussi, *J. Phys. Chem. C* 2007, **111**, 11528.
21. J. Wang, P. Jiang, L. Gao, Y. Yu, Y. Lu, L. Qiu, C. Wang and J. Xia, *J. Nanopart. Res.* 2013, **15**, 1914.
22. Y. Li, L. Guan, H. Zhang, J. Chen, S. Lin, Z. Ma and Y. Zhao, *Anal. Chem.* 2011, **83**, 4103.

23. I. L. Medintz, A. R. Clapp, H. Mattoussi, E. R. Goldman, B. Fisher and J. M. Mauro, *Nat. Mater.* 2003, **2**, 630.
24. S. K. Gunasekar, M. Asnani, C. Limbad, J. S. Haghpanah, W. Hom, H. Barra, S. Nanda, M. Lu and J. K. Montclare, *Biochemistry* 2009, **48**, 8559.
25. W, Shen, K. C. Zhang, J. A. Kornfield and D. A. Tirrell, *Nat. Mater.* 2006, **5**, 153.
26. B. Liu, A. K. Lewis and W. Shen, *Biomacromolecules* 2009, **10**, 3182.
27. E. Fong and D. A. Tirrell, *Adv. Mater.* 2010, **22**, 5271.
28. J. B. Delehanty, H. Mattoussi and I. L. Medintz, *Anal. Bioanal. Chem.* 2009, **393**, 1091.
29. A. V. Kabanov and S. V. Vinogradov, *Angew. Chem. Int. Ed.* 2009, **48**, 5418.
30. B. Liu, X. Hu, J. Liu, Y. Zhao, Z. Huang and Q. Luo, *Tetrahedron Lett.* 2007, **48**, 5958.
31. W. A. Petka, J. L. Harden, K. P. McGrath, D. Wirtz and D. A. Tirrell, *Science* 1998, **281**, 389.
32. C. K. Kim, P. Ghosh, C. Pagliuca, Z. Zhu, S. Menichetti and V. M. Rotello, *J. Am. Chem. Soc.* 2009, **131**, 1360.
33. J. Du, X. Du, C. Mao and J. Wang, *J. Am. Chem. Soc.* 2011, **133**, 17560.
34. J. Wang and J. Xia, *Anal. Chem.* 2011, **83**, 6323.
35. L. Xiong, Z. Chen, Q. Tian, T. Cao, C. Xu and F. Li, *Anal. Chem.* 2009, **81**, 8687.
36. A. Celik, U. Comelekoglu and S. Yalin, *Toxicol. Ind. Health* 2005, **21**, 243.
37. H. Zhang, Y. Li, J. Wang, X. Li, S. Lin, Y. Zhao and Q. Luo, *J. Biomed. Opt*. 2010, **15**, 015001.
38. J. Pan, and S. Feng, *Biomaterials* 2009, **30**, 1176.
39. T. Liu, Z. Huang, H. Wang, J. Wang, X. Li, Y. Zhao and Q. Luo, *Anal. Chim. Acta* 2006, **559**, 120.
40. W. W. Yu, L. Qu, W. Guo and X. Peng, *Chem. Mater.* 2003, **15**, 2854.
41. D. Magde, R. Wong and P. G. Seybold, *Photochem. Photobiol.* 2002, **75**, 327.

